

The atypical iron-coordination geometry of cytochrome *f* remains unchanged upon binding to plastocyanin, as inferred by XAS

Irene Díaz-Moreno · Sofía Díaz-Moreno ·
Gloria Subías · Miguel A. De la Rosa ·
Antonio Díaz-Quintana

Received: 8 July 2006 / Accepted: 25 August 2006 / Published online: 17 November 2006
© Springer Science+Business Media B.V. 2006

Abstract The transient complex between cytochrome *f* and plastocyanin from the cyanobacterium *Nostoc* sp. PCC 7119 has been analysed by X-ray Absorption Spectroscopy in solution, using both proteins in their oxidized and reduced states. Fe K-edge data mainly shows that the atypical metal coordination geometry of cytochrome *f*, in which the N-terminal amino acid acts as an axial ligand of the heme group, remains unaltered upon binding to its redox partner, plastocyanin. This fact suggests that cytochrome *f* provides a stable binding site for plastocyanin and minimizes the reorganization energy required in the transient complex formation, which could facilitate the electron transfer between the two redox partners.

Keywords Cytochrome *f* · Electron transfer · Metalloproteins · Plastocyanin · Transient complexes · X-ray absorption spectroscopy

Abbreviations

Cf	water-soluble fragment of cytochrome <i>f</i>
ET	electron transfer
EXAFS	extended X-ray absorption fine structure
FT	Fourier transform
Pc	plastocyanin
XANES	X-ray absorption near edge structure
XAS	X-ray absorption spectroscopy
XRD	X-Ray diffraction
ΔE_0	internal potential correction
Δr	change in the distance between the metal and ligand atoms
σ	Debye–Waller parameter related to the system dynamic disorder

I. Díaz-Moreno · M. A. De la Rosa · A. Díaz-Quintana
Instituto de Bioquímica Vegetal y Fotosíntesis, Universidad de Sevilla y Consejo Superior de Investigaciones Científicas, Américo Vespucio 49, 41092 Sevilla, Spain

S. Díaz-Moreno
Rutherford Appleton Laboratory, Diamond Light Source Ltd., Chilton, Didcot, Oxfordshire OX11 0QX, UK

G. Subías
Departamento de Física de la Materia Condensada, Instituto de Ciencia de Materiales de Aragón, Universidad de Zaragoza y Consejo Superior de Investigaciones Científicas, Plaza San Francisco s/n, 50009 Zaragoza, Spain

I. Díaz-Moreno (✉)
National Institute for Medical Research, Molecular Structure Division, The Ridgeway, Mill Hill, NW7 1AA London, UK
e-mail: irene.diazmoreno@nimr.mrc.ac.uk

Introduction

In oxygen-evolving photosynthetic organisms, the cytochrome *b₆-f* complex couples proton translocation across the thylacoid membrane to the electron transport between photosystems I and II (Allen 2004). In this complex, cytochrome *f* (Cf) transfers electrons from the Rieske iron sulphur cluster to a soluble metalloprotein that acts as the immediate electron donor of P700 cofactor at Photosystem I.

The Cf subunit consists on a 28.2 kDa N-terminal soluble domain anchored to the membrane by C-terminal helix (Gray 1992). Its soluble domain is an

atypical *c*-type cytochrome because both its β -sheet secondary structure and the unusual heme axial coordination (Martinez et al. 1994) with the N-terminal amino acid Tyr-1 acting as an axial ligand.

The most ubiquitous electron carrier between *Cf* and P700 is plastocyanin (Pc) (Sandman et al. 1983), which is a type I cupredoxin (Gough and Chotia 2004). Its structure consists on an anti-parallel β -barrel with a single copper atom (Coleman et al. 1978; Sykes 1985; Redinbo et al. 1994) coordinated by two nitrogen atoms and two sulphur ones from highly conserved residues (H39, C89, H92 and M97 in *Nostoc* cyanobacterium).

The mechanism of the electron transfer (ET) reaction between Pc and its physiological partners has been studied extensively (Hope 2000; Hervás et al. 2003; Díaz-Quintana et al. 2003) highlighting the role of electrostatic and hydrophobic interactions on binding. Also, the solution structures of several Pc–*Cf* complexes have been reported (Ubbink 2004; Díaz-Moreno et al. 2005a, Lange et al. 2005; Musiani et al. 2005). In all the cases, these structures are consistent with a single conformation ensemble in which the hydrophobic patch surrounding Tyr-1 in *Cf* docks the hydrophobic patch of Pc.

Despite the large amount of data concerning the nature of the interactions influencing the binding between the redox partners, little is known about the effects of complex formation on the metal cofactors, and how they can modulate the ET process. An analysis about whether the Fe coordination in *Cf* is altered upon binding to Pc would be interesting to address the above-mentioned effects, especially due to the fact that the N-terminal amino acid Tyr-1, which is involved in the Pc–*Cf* interface (Ubbink 2004; Díaz-Moreno et al. 2005a, Lange et al. 2005; Musiani et al. 2005), acts as axial ligand. To get a deep insight on these subjects we have studied the Fe K-edge of free and Pc-bound *Cf* by X-ray absorption spectroscopy (XAS) in solution.

Materials and methods

Protein samples

Nostoc sp. PCC 7119 Pc was purified from *E. coli* cells transformed with the pEAP-WT plasmid (Molina-Heredia et al. 1998). Production and purification of the soluble domain of *Nostoc* sp. PCC 7119 *Cf* were as previously described (Albarrán et al. 2005).

For the XAS experiments, the Pc and *Cf* samples were concentrated to the required volume by ultrafil-

tration methods, and exchanged into 10 mM sodium phosphate pH 6.0. After concentration, stock solutions of 10 mM Pc and 4.5 mM *Cf* were obtained. Protein concentration was determined by optical spectroscopy using an absorption coefficient of $4.5 \text{ mM}^{-1} \text{ cm}^{-1}$ at 598 nm for oxidized Pc (Molina-Heredia et al. 1998) and $31.5 \text{ mM}^{-1} \text{ cm}^{-1}$ at 556 nm for reduced *Cf* (Albarrán et al. 2005). Oxidized *Cf* (Cf^{III}) was prepared by adding an equimolecular amount of potassium ferricyanide, followed by gel filtration in a Pharmacia Superdex G75 column to remove ferrocyanide. Reduced *Cf* (Cf^{II}) was obtained upon addition of a tenfold excess of sodium ascorbate to a resulting Cf^{III} sample. Oxidized Pc (Pc^{II}) was obtained by addition of either ferricyanide, as described for *Cf*. The oxidized complex ($\text{Pc}^{\text{II}}\text{--}\text{Cf}^{\text{III}}$) was prepared by adding an aliquot of a 10 mM Pc^{II} onto a Cf^{III} sample up to reach a final concentration of ca. 2 mM each. Under these conditions, the percentage of Pc bound to *Cf* was estimated to be ca. 87%, according to the binding constant calculated from NMR data (Díaz-Moreno et al., 2005a). The reduced complex ($\text{Pc}^{\text{I}}\text{--}\text{Cf}^{\text{II}}$) was obtained upon addition of a tenfold excess of sodium ascorbate to a $\text{Pc}^{\text{II}}\text{--}\text{Cf}^{\text{III}}$ sample prepared as above.

XAS measurements

The X-ray absorption spectra were recorded at the European Synchrotron Radiation Facility (ESRF) in Grenoble (France), which was operating with a ring current of 200 mA and energy of 6 GeV. The Fe K-edge (7112 eV) was measured at beam line BM29 using a double crystal monochromator fitted with a pair of flat Si (311) crystals detuned to 50% fwhm of the maximum transmission, for the suppression of high energy harmonics.

All measurements were made at room temperature in fluorescence mode, using a 13-element Canberra solid-state germanium detector. The samples were contained in a PTFE cell equipped with two 12 μm Kapton foil windows.

Energy calibration was achieved by measuring an iron foil for the Fe edge. The spectra of the foil were measured simultaneously, with the data in transmission mode, to be used as an internal reference. Ionization chambers filled with the appropriate mixture of gases were used as detectors.

For all measurements, each data point was collected for 4 s, and several scans were averaged to achieve a good signal-to-noise ratio. In no case protein photo-reduction or damage was observed, even in those samples in which the measurements were made over several hours. For the oxidized forms free and

Pc-bound Cf , the edge remained at fix energy position from the first to the last scan, thus confirming the absence of protein photoreduction. The lack of radiation-induced changes in the samples was also confirmed by UV-vis measurements before and after XAS measurements.

XAS data analysis

The background subtraction required to obtain the extended X-ray absorption fine structure (EXAFS) functions $\chi(k)$ from the measured X-ray absorption spectra were performed using the AUTOBK code from the University of Washington. E_0 was defined as the maximum of the first derivative of the absorption edge.

To analyze the EXAFS spectra, the theoretical phases and amplitudes were calculated using the FEFF 6.0 code (Rehr et al. 1992; Newville et al. 1995). The fit to the experimental data was performed using the FEFFIT program (version 2.54) (Newville et al. 1995).

Results and discussion

XANES region

Figure 1 (*upper panel*) shows the X-ray absorption near edge structure (XANES) spectra corresponding to free Cf in its reduced and oxidized states. In both spectra there is a pre-edge feature corresponding to the forbidden transition $1s-3d$, which is sensitive to the electronic and geometric structure of the atom (Fe) site (Westre et al. 1997). In fact, the intensity of this transition agrees with the octahedral environment around the iron atom in Cf (Martinez et al. 1994).

On the other hand, the edge position, determined by the maximum in the first derivative of the absorption spectrum corresponding to free Cf^{II} , appears ca. 1 eV below that of Cf^{III} , as previously found for the reduced and oxidized states of two closely related proteins, as heart cytochrome *c* (Cheng et al. 1999) and *Nostoc* cytochrome *c*₆ (Díaz-Moreno et al. 2006). In case of cytochrome *c* (Cheng et al. 1999), photoreduction of the oxidized species was observed only after the 16th spectrum of the series. In our case, however, there is no photoreduction as inferred from the fact that the edge position remains fixed for all the spectra along each series i.e. reduced or oxidized, free or bound. The reason not to observe any sample photo-reduction is due to the moderate brightness of the EXAFS spectrometer deliberately chosen for this investigation. In addition, the same shift has also been reported upon

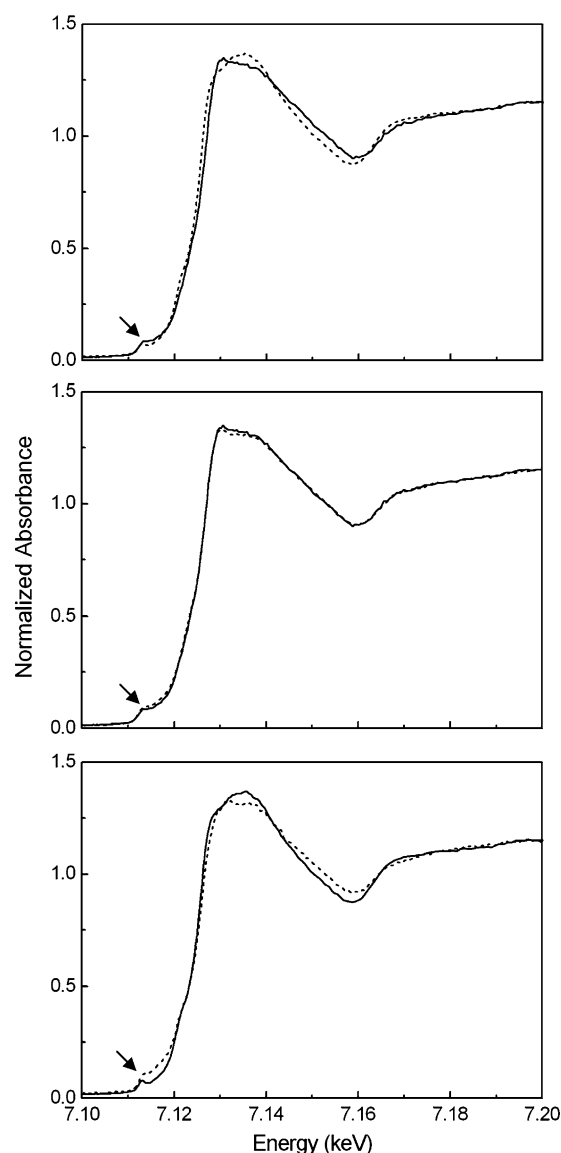


Fig. 1 XANES region of the Fe K-edge XAS spectra of free and Pc-bound Cf . *Upper*, experimental data for oxidized and reduced forms of free proteins, Cf^{III} (continuous line) and Cf^{II} (dashed line). *Middle*, data for the oxidized species, Cf^{III} (continuous line) and $Pc^{II}-Cf^{III}$ complex (dashed line). *Lower*, data for the reduced species, Cf^{II} (continuous line) and Pc^I-Cf^{II} complex (dashed line). The presence of a pre-edge signal at 7113 eV is marked by arrows

oxidation from Fe^{2+} to Fe^{3+} at pH 7 in the heme protein cytochrome *c* (Shulman et al. 1976).

Moreover, there are some differences in both XANES spectra, particularly in the first feature after the edge.

Figure 1 also shows the XANES regions of the absorption spectra of Cf bound to Pc in the oxidized and reduced state. The XANES region of the absorption spectra for $Pc^{II}-Cf^{III}$ and Cf^{III} are identical (Fig. 1, *middle panel*), indicating that the electronic

and geometrical configuration around the iron centre remains unchanged when bound to Pc. However, this is not the case for the reduced proteins (Fig. 1, lower panel). In fact, the spectrum of the $\text{Pc}^{\text{I}}\text{-Cf}^{\text{II}}$ complex exhibits some differences compared with that of free Cf^{II} . With regard to the pre-edge, a slight increase in the intensity of this feature is observed for Cf^{II} when bound to Pc^{I} , according to the decrease in electron density of the Fe atom. The shape of the first feature after the edge slightly changes too, thus suggesting certain modifications in the geometrical distribution of the ligands around the iron atom. It is worth noting that the spectrum of the reduced complex is very similar—except for the pre-edge signal and edge position—to that of the oxidized complex and free oxidized Cf, as shown in Fig. 3. This suggests that the iron geometry in reduced Cf is distorted upon association to Pc, approaching to that of the iron centre in the oxidized form, either free or bound to Pc.

EXAFS Region

The extracted EXAFS signals of Cf in the reduced and oxidized states are shown in Fig. 2 (left panels) as k -weighted spectra. The choice of a k -weighting instead of a k^3 -weighting is based on the following facts. First, we were interested in determining the local environment around the absorbing atom and, in particular, at the first coordination shell. This shell is formed by iron and light elements, such as nitrogen, and their backscattering amplitude drops quickly at increasing energy (k value). Therefore, they have a larger contribution when the transforms are made in k rather than in k^3 . Second, if a k^3 -weighting is used, the highest energy part of the spectrum is emphasized and, in this case, the EXAFS signal would be dominated by the spectral region where the signal-to-noise ratio is poorer.

We should note here that the XAS data were collected at room temperature in order to maintain consistency with previous room temperature NMR measurements made on the same systems (Díaz-Moreno et al. 2005a, b). Although a better signal to noise should be obtained at cryogenic temperatures, the transient complexes we study are not stable upon freezing, unless the partners are chemically cross-linked. Similar experimental conditions are required by EPR. Although EPR measurements on free and Pc-bound Cf would help to study the iron geometry, any comparison between results inferred from NMR or XAS, on one hand, and EPR, on the other, would be unreliable.

As can be seen, the EXAFS function is not a simple wave but a combination of different waves

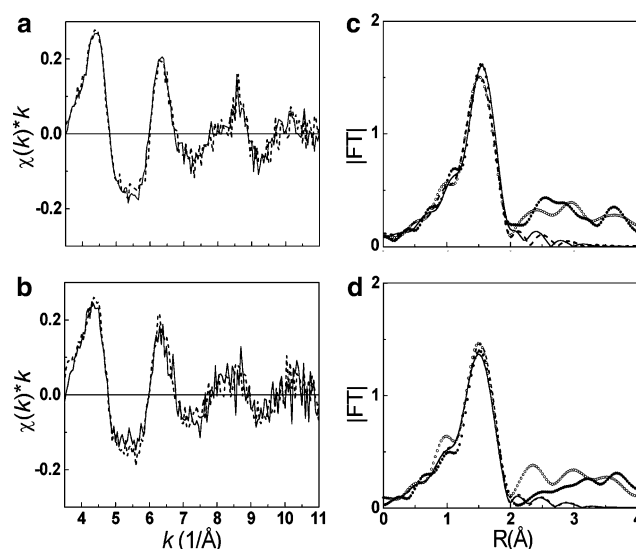


Fig. 2 EXAFS data (panels a and b) and their FT modules (panels c and d) at the Fe K-edge of Cf, either free or bound to Pc. The EXAFS spectra of free proteins (Cf^{II} and Cf^{III}) are shown in **panel a** by continuous line for Cf^{II} and dashed line for Cf^{III} . In **panel b**, the EXAFS spectra of $\text{Pc}^{\text{I}}\text{-Cf}^{\text{II}}$ and $\text{Pc}^{\text{II}}\text{-Cf}^{\text{III}}$ complexes are represented by continuous and dashed lines, respectively. The corresponding FT modules of the EXAFS spectra for free Cf (Cf^{II} and Cf^{III}) are represented in **panel c** by closed and open circles, respectively. **Panel d** shows the FT modules for Pc-bound Cf forms: $\text{Pc}^{\text{I}}\text{-Cf}^{\text{II}}$ by closed circles and $\text{Pc}^{\text{II}}\text{-Cf}^{\text{III}}$ by open circles. The best fits of the FT data for both reduced (Cf^{II} and $\text{Pc}^{\text{I}}\text{-Cf}^{\text{II}}$) and oxidized states (Cf^{III} and $\text{Pc}^{\text{II}}\text{-Cf}^{\text{III}}$) are represented by continuous and dashed lines, respectively

corresponding to the contributions from the neighbouring atoms at different distances around the iron centre. Indeed, the EXAFS signals of Cf do not change upon binding to Pc, thereby indicating that the local coordination environment around the iron centre remains unchanged.

The Fourier Transform (FT) of the corresponding spectra and the best fits, obtained with the parameters included in Table 1, are also shown in Fig. 2 (right panels). As a starting model, the values obtained from the X-ray diffraction (XRD) structure of *Phormidium* Cf (Carrel et al. 1999) were used. In all cases there is a main signal around 1.5 Å, which corresponds to the first coordination sphere formed by the four nitrogen atoms of the porphyrin ring (NA, NB, NC and ND), along with the nitrogen atoms of the two iron axial ligands Tyr-1 (N) and His-26 (N_{e2}). The intensities of the remaining signals are significantly lower than the first one because they correspond to contributions from lightweight elements lying at longer coordination distances. In order to fit the data, six simple scattering paths from the Fe atom to the six ligand N atoms were selected. Δr_1 and Δr_2 were used as two fitting

parameters corresponding to changes in the distances of Fe to the two axial N atoms and to the four porphyrin N atoms, respectively. The Debye–Waller parameter, σ^2 , related to system dynamic disorder was also fitted, with σ_1^2 accounting for the bonds between the Fe atom and the two axial N atoms and σ_2^2 accounting for the bonds between the Fe atom and the four porphyrin N atoms. The fifth adjustable parameter was the internal potential correction (ΔE_0).

Although there are no significant changes in the metal–ligand distances, the Fe K-edge X-ray absorption data suggests a small distortion of the Fe^{2+} metal centre geometry when Cf^{II} binds to Pc^{I} . The resulting Fe^{2+} geometry resembles that of Cf^{III} , either free or bound to Pc^{II} (Fig. 3). Although the Fe atom of Cf shows a well-defined position at the heme group, which provides a rigid frame, the small distortion on the Fe^{2+} metal centre when Cf^{II} binds to Pc^{I} can be explained by the smaller size of Fe^{3+} compared to Fe^{2+} : The Fe^{3+} atom fits well into the heme ring whereas the Fe^{2+} atom is somewhat shifted out of the plane (Schnackenberg et al. 1999); however, the Fe^{2+} atom could be driven into the ring upon complex formation, thus yielding a structure of Pc^{I} -bound Fe^{2+} similar to that of Fe^{3+} in free and Pc^{II} -bound Cf^{III} .

Table 1 Best-fit structural parameters resulted from the EXAFS analysis for free and Pc-bound Cf, in both oxidized and reduced state

System	Ligand	ΔE_0 (eV)	$r(\text{M-L})$ (Å)	$\sigma^2(\text{M-L})$ (Å ²)
Cf^{III}	N (NC)	-7 ± 4	1.96 ± 0.02	0.002 ± 0.001
	N (NA & ND)		1.97 ± 0.02	
	N (NB)		1.98 ± 0.02	
	N (N_{e2})		2.44 ± 0.06	
	N (N)		2.49 ± 0.06	
Cf^{II}	N (NC)	-6 ± 2	1.97 ± 0.01	0.002 ± 0.001
	N (NA & ND)		1.99 ± 0.01	
	N (NB)		2.00 ± 0.01	
	N (N_{e2})		2.43 ± 0.02	
	N (N)		2.48 ± 0.02	
$\text{Pc}^{\text{II}}\text{-Cf}^{\text{III}}$	N (NC)	-7 ± 3	1.97 ± 0.01	0.002 ± 0.001
	N (NA & ND)		1.98 ± 0.01	
	N (NB)		1.99 ± 0.01	
	N (N_{e2})		2.40 ± 0.03	
	N (N)		2.45 ± 0.03	
$\text{Pc}^{\text{I}}\text{-Cf}^{\text{II}}$	N (NC)	-6 ± 3	1.97 ± 0.02	0.003 ± 0.001
	N (NA & ND)		1.98 ± 0.02	
	N (NB)		1.99 ± 0.02	
	N (N_{e2})		2.40 ± 0.03	
	N (N)		2.45 ± 0.03	

S_0^2 , factor of amplitude of reduction; $r(\text{M-L})$, metal–ligand distance

$S_0^2 = 1.0$, $\Delta k = 3.5\text{--}11$ (1/Å), $\Delta R = 1.1\text{--}2.1$ (Å), R factor (free Cf^{III}) = 0.044, R factor (free Cf^{II}) = 0.004, R factor (Pc^{II} -bound Cf^{III}) = 0.004, R factor (Pc^{I} -bound Cf^{II}) = 0.003

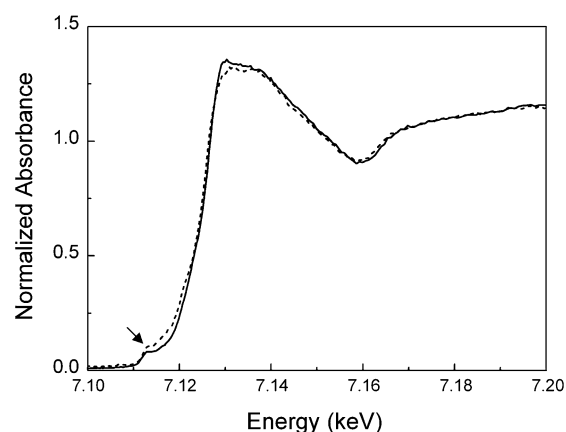


Fig. 3 XANES region of the Fe K-edge XAS spectra of free Cf^{III} and Pc^{I} -bound Cf^{II} . Experimental data for Cf^{III} and $\text{Pc}^{\text{I}}\text{-Cf}^{\text{II}}$ are shown in continuous and dashed lines. The presence of a pre-edge signal at 7113 eV is marked by arrows

This tiny perturbation is consistent with the intensity changes at the pre-edge region of Cf^{II} in presence of Pc^{I} , because they correspond to transitions to the iron d_{z^2} and $d_{x^2-y^2}$ orbitals, which are pointing towards the axial and equatorial ligands, respectively. As the reducing electron is not located in these orbitals, such subtle changes may have little influence on the redox potential. This situation is clearly different to that previously reported for cytochrome c_6 , which shows a perturbation on the pre-edge region corresponding to its oxidized species, instead of the reduced ones, upon binding its reaction partner, photosystem I (Díaz-Moreno et al. 2006). In such case the pre-edge corresponds to transfer to a half-occupied non-bonding d orbital, which is that receiving the reducing electron, so the observed changes can be correlated with changes in the redox potential of the heme protein. Regarding to this point, it is important to note that the heme plane is normal to the interaction surface of cytochrome c_6 , but parallel in the case of Cf.

Thus, our results indicate that the bond between iron and the N-terminus nitrogen is strong enough to prevent a distortion of the iron-coordination geometry upon binding of Cf to Pc, as well as to provide a stable binding site to the copper protein. Such a stiffness of the coordination sphere minimises the reorganisation energy concomitant to charge transfer, thus optimising the ET process.

Acknowledgements This work was supported by the European Synchrotron Radiation Facility (ESRF SC-1366), the Spanish Ministry of Education and Science (AP2000-2937, BMC2003-00458 and MAT02-01221) and the Andalusian Government (PAI, CVI-0198).

References

- Albarrán C, Navarro JA, Molina-Heredia FP, Murdoch PS, De la Rosa MA, Hervás M (2005) Laser flash-induced kinetic analysis of cytochrome *f* oxidation by wild-type and mutant plastocyanin from the cyanobacterium *Nostoc sp* PCC 7119. *Biochemistry* 44:11601–11607
- Allen JF (2004) Cytochrome *b₆f*: structure for signalling and vectorial metabolism. *Trends Plant Sci* 9:130–137
- Carrel CJ, Schlarb BG, Bendall DS, Howe CJ, Cramer WA, Smith JL (1999) Structure of the soluble domain of cytochrome *f* from the cyanobacterium *Phormidium laminosum*. *Biochemistry* 38:9590–9599
- Cheng MG, Rich AM, Armstrong RS, Ellis PJ, Lay PA (1999) Determination of iron-ligand bond lengths in ferric and ferrous horse heart cytochrome *c* using multiple-scattering analyses of XAFS data. *Inorg Chem* 38:5703–5708
- Coleman PM, Guss JM, Sugimura Y, Yoshizaki FY, Freeman HC (1978) Crystal structure of plastocyanin from a green alga, *Enteromorpha prolifera*. *J Mol Biol* 211:617–632
- Díaz-Moreno I, Díaz-Quintana A, De la Rosa MA, Ubbink M (2005a) The orientation of plastocyanin in the complex with cytochrome *f* from the cyanobacterium *Nostoc* determined by paramagnetic NMR. *J Biol Chem* 280:18908–18915
- Díaz-Moreno I, Díaz-Quintana A, De la Rosa MA, Crowley PB, Ubbink M (2005b) Different modes of interaction in cyanobacterial complexes of plastocyanin and cytochrome *f*. *Biochemistry* 44:3176–3183
- Díaz-Moreno I, Díaz-Quintana A, Subías G, Mairs T, De la Rosa MA, Díaz-Moreno S (2006) Detecting transient protein-protein interactions by X-ray absorption spectroscopy: the cytochrome *c₆*-photosystem I complex. *FEBS Lett* 580:3023–3028
- Díaz-Quintana A, Navarro JA, Hervás M, Molina-Heredia FP, De la Cerda B, De la Rosa MA (2003) A comparative structural and functional analysis of cyanobacterial plastocyanin and cytochrome *c₆* as alternative electron donors to Photosystem I. *Photosynth Res* 75:97–110
- Gough J, Chotia C (2004) The linked conservation of structure and function in a family of high diversity: The monomeric cupredoxins. *Structure* 12:917–925
- Gray JC (1992) Cytochrome *f*: structure, function and biosynthesis. *Photosynth Res* 34:359–374
- Hervás M, Navarro JA, De la Rosa MA (2003) Electron Transfer between Membrane Complexes and Soluble Proteins in Photosynthesis. *Acc Chem Res* 36:798–805
- Hope AB (2000) Electron transfers amongst cytochrome *f*, plastocyanin and photosystem I: Kinetics and mechanisms. *Biochim Biophys Acta* 1456:5–26
- Lange C, Cornvik T, Díaz-Moreno I, Ubbink M (2005) The transient interaction of poplar plastocyanin with cytochrome *f* studied by 2D-NMR spectroscopy: effects of ionic strength and pH. *BBA Bioenergetics* 1707:179–188
- Martinez SE, Huang M, Szczepaniak A, Cramer WA, Smith JL (1994) Crystal structure of chloroplast cytochrome *f* reveals a novel cytochrome fold and unexpected heme ligation. *Structure* 2:95–105
- Molina-Heredia FP, Hervás M, Navarro JA, De la Rosa MA (1998) Cloning and correct expression in *Escherichia coli* of the *petE* and *petJ* genes respectively encoding plastocyanin and cytochrome *c₆* from the cyanobacterium *Anabaena sp.* PCC 7119. *Biochem Biophys Res Commun* 243:302–306
- Musiani F, Dikii A, Semenov AY, Ciurli S (2005) Structure of the intermolecular complex between plastocyanin and cytochrome *f* from spinach. *J Biol Chem* 280:18883–18841
- Newville M, Ravel B, Haskel D, Rehr JJ, Stern EA, Yacoby Y (1995) Analysis of multiple-scattering XAFS data using theoretical standards. *Physica B* 208&209:154–155
- Redinbo MR, Yeates TO, Merchant S (1994) Plastocyanin: structural and functional analysis. *J Bioenerg Biomembr* 26:49–66
- Rehr JJ, Zabinsky SI, Albers RC (1992) High-order multiple scattering calculations of x-ray-absorption fine structure. *Phys Rev Lett* 69:3397–3401
- Sandman G, Reck H, Kessler E, Böger P (1983) Distribution of plastocyanin and soluble plastidic cytochrome *c* in various classes of algae. *Arch Microbiol* 134:23–27
- Schnackenberg J, Than ME, Mann K, Wiegand G, Huber R, Reuter W (1999) Amino acid sequence, crystallization and structure determination of reduced and oxidized cytochrome *c₆* from the green alga *Scenedesmus obliquus*. *J Mol Biol* 290:1019–1030
- Shulman RG, Yafet T, Eisenberger P, Blumberg WE (1976) Observation and interpretation of X-ray absorption edges in iron compounds and proteins. *Proc Natl Acad Sci USA* 73:1384–1388
- Sykes AG (1985) Tilden Lecture: Structure and Electron-transfer Reactivity of the Blue Copper Protein Plastocyanin. *Chem Soc Rev* 14:283–315
- Ubbink M (2004) Complexes of photosynthetic redox proteins studied by NMR. *Photosynth Res* 81:277–287
- Westre TE, Kennepohl P, DeWitt JG, Hedman B, Hodgson KO, Solomon E (1997) A multiplet analysis of the Fe K-edge 1s-3d pre-edge features of iron complexes. *J Am Chem Soc* 119:6297–6314